Cytosol Has a Small Effect on Protein Backbone Dynamics†

Julie E. Bryant,‡,§ Juliette T. J. Lecomte,|| Andrew L. Lee,⊥,@,# Gregory B. Young,@ and Gary J. Pielak*,‡,@,#

Department of Chemistry, Department of Biochemistry and Biophysics, Division of Medicinal Chemistry and Natural Products, and Lineberger Comprehensive Cancer Research Center, University of North Carolina, Chapel Hill, North Carolina 27599, and Department of Chemistry, The Pennsylvania State University, University Park, Pennsylvania 16802

Received March 18, 2006; Revised Manuscript Received June 16, 2006

ABSTRACT: Cells are crowded with macromolecules, yet most biophysical information about proteins is obtained in dilute solution. To determine the impact of this dichotomy, we used nuclear magnetic resonance spectroscopy to measure the backbone ^{15}N T_1 and T_2 relaxation times and the $\{^1H\}-^{15}N$ nuclear Overhauser enhancement (nOe) of uniformly ^{15}N-enriched apocytochrome b_5 in living *Escherichia coli* and in dilute solution. These data allowed us to assess the backbone dynamics of this partially folded protein in cells and in dilute solution. The two data sets were analyzed by using the model-free approach. Transfer from dilute solution to the cytosol has a quantitative effect on T_1, T_2, and nOe values. Most of the effects are attributed to an increase in the overall correlation time, caused by the increased viscosity of the cytosol compared to that of the dilute solution. Our main conclusion is that the cytosol does not alter the pattern of backbone dynamics of apocytochrome b_5. Increases in the time scale of both the picosecond and millisecond motions are observed, but the increases are less than ∼30%.

Proteins catalyze nearly all of a cell's chemical reactions, and they do so under tightly packed conditions. The cytosol is extremely crowded, in large part because of proteins themselves occupying 40% of a cell's volume and reaching concentrations of >300 g/L (*1*). Such macromolecular crowding can affect protein structure (*2*, *3*), association (*4*), and stability (*5*), yet almost all biophysical studies of proteins are performed in dilute solution. In recent years, in-cell NMR spectroscopy (*6*, *7*) has opened the door to atomic-level studies of protein chemistry under conditions close to physiological.

We reported the first measurements of fast backbone dynamics in living cells based on the $\{^1H\}-^{15}N$ nuclear Overhauser enhancement (nOe)[1] experiment (*8*). These data show that the average structure of the test protein, apocytochrome b_5, does not change when it is transferred from a dilute solution to the cytosol of *Escherichia coli* and that the picosecond to nanosecond backbone dynamics are similar in dilute solution and in cells. A complete study of fast dynamics, however, requires additional measurements. Here, ^{15}N T_1 and T_2 relaxation times are reported both in cells and in dilute solution. These data are combined with the nOe data to provide a more complete picture. In the remainder of the introductory section, we describe three subjects: apocytochrome b_5, NMR-detected fast backbone dynamics, and analysis of these data.

Removing the noncovalently bound heme from the 98-residue water-soluble domain of cytochrome b_5 produces apocytochrome b_5. In solution, this 11.2 kDa globular protein (Figure 1) is disordered at the termini and in the heme-binding loop (*9*). We chose apocytochrome b_5 for studies of in-cell protein dynamics for two reasons. First, its structure, as described by ^1H and ^{15}N chemical shifts, does not change when it is transferred from dilute solution to the inside of cells (*8*). Second, its partially folded nature provides a rich landscape of backbone dynamics that has already been extensively studied in dilute solution with NMR (*10*, *11*).

The major mechanisms that allow ^{15}N magnetic relaxation are the dipolar coupling of the ^{15}N nucleus to its bound ^1H and the ^{15}N chemical shift anisotropy (due to the unsymmetrical electron distribution in the H−N bond) (*12*). This relaxation occurs because molecular motions generate local magnetic fields at appropriate frequencies. The longitudinal (T_1) relaxation time and the $\{^1H\}-^{15}N$ nOe are affected by fast, picosecond to nanosecond, motions. Both fast and slower motions can be investigated by measuring the transverse (T_2) relaxation time of the ^{15}N nucleus.

† This work was supported by the National Science Foundation (Grants MCB 0212939 and 0516547 to G.J.P.), the Petroleum Research Fund (Grant 42748-AC4 to G.J.P.), and the National Institutes of Health (Grant GM-54217 to J.T.J.L.). J.E.B. was partially supported by a Dobbins Fellowship.

* To whom correspondence should be addressed: Department of Chemistry, University of North Carolina, Chapel Hill, NC 27599. Phone: (919) 966-3671. Fax: (919) 966-3675. E-mail: gary_pielak@unc.edu.

‡ Department of Chemistry, University of North Carolina.

§ Present address: Schering-Plough Research Institute, 2015 Galloping Hill Road, K-15, B307C, Kenilworth, NJ 07033.

|| Department of Chemistry, The Pennsylvania State University.

⊥ Division of Medicinal Chemistry and Natural Products, University of North Carolina.

@ Department of Biochemistry and Biophysics, University of North Carolina.

Lineberger Comprehensive Cancer Research Center, University of North Carolina.

[1] Abbreviations: $J(\omega)$, spectral density at frequency ω; nOe, nuclear Overhauser enhancement; R_{ex}, relaxation due to motions much slower than molecular tumbling; S^2, square of the order parameter indicating the restriction of the motion experienced by a $^1H-^{15}N$ vector; T_1, longitudinal relaxation time; T_2, transverse relaxation time; τ_e, internal effective correlation time; τ_m, overall rotational correlation time for isotropic tumbling.

10.1021/bi060547b CCC: $33.50
Published on Web 08/01/2006

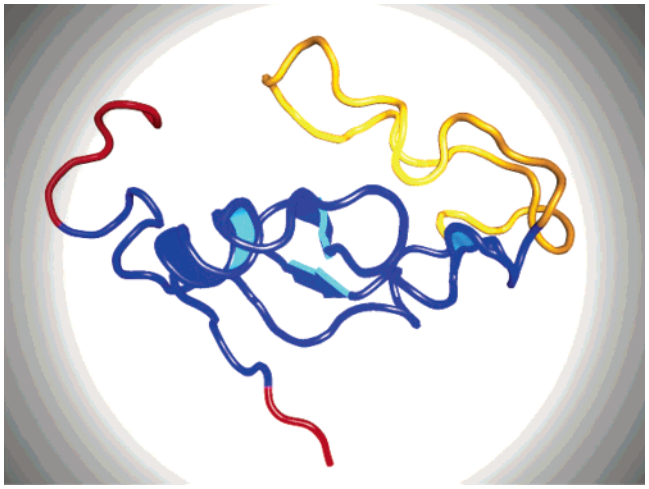

FIGURE 1: Apocytochrome b_5 average NMR solution structure (Protein Data Bank entry 1I87). The well-defined regions of the average structure (*10*) are colored blue; the heme-binding loop is at the top and colored yellow, and the disordered termini are colored red. The rendering was made with MacPyMOL (*31*).

The spectral density function, $J(\omega)$, describes the probability of finding a component of the molecule's motions at a specific frequency, ω (*13*). Equations 1−3 describe the linear combinations of frequency distributions required for ^{15}N relaxation (*13*).

$$\frac{1}{T_1} = \frac{d^2}{4}[J(\omega_H - \omega_N) + 3J(\omega_N) + 6J(\omega_H + \omega_N)] + c^2 J(\omega_N) \quad (1)$$

$$\frac{1}{T_2} = \frac{d^2}{8}[4J(0) + J(\omega_H - \omega_N) + 3J(\omega_N) + 6J(\omega_H) + 6J(\omega_H + \omega_N)] + \frac{c^2}{6}[3J(\omega_N) + 4J(0)] + R_{ex} \quad (2)$$

$$\text{nOe} = 1 + \frac{\gamma_H}{\gamma_N}\frac{d^2}{4}[6J(\omega_H + \omega_N) - J(\omega_H - \omega_N)]\frac{1}{T_1} \quad (3)$$

where $c^2 = (\Delta\sigma\omega_N/\sqrt{3})^2$, $d^2 = ([\mu_0\gamma_H\gamma_N h/(8\pi^2)]\langle r_{NH}^{-3}\rangle)^2$, $\Delta\sigma$ is the chemical shift anisotropy (160 ppm), μ_0 is the permeability of free space, γ_H and γ_N are the gyromagnetic ratios for ^{1}H and ^{15}N, respectively, h is Planck's constant, and r_{NH} is the internuclear ^{1}H−^{15}N distance (1.02 Å).

The longitudinal relaxation and the {^{1}H}−^{15}N nOe depend on motions with components at the high Larmor frequencies of ^{1}H (ω_H) and ^{15}N (ω_N) nuclei, which in turn depend on the applied static magnetic field, B_0. These frequencies are in the megahertz range. The $J(0)$ and R_{ex} terms in the equation for T_2 indicate additional sensitivity to slower motions. The difference between $J(0)$ and $J(\omega_N)$ becomes increasingly pronounced when the molecular tumbling correlation time increases above a few nanoseconds, and when R_{ex} contributes to T_2 via chemical-exchange processes on the microsecond to millisecond time scale (*11*, *13*).

Lipari and Szabo (*14*, *15*) introduced a "model-free" analysis that assumes a simple Lorentzian form for the spectral density function $J(\omega)$ and allows separation of internal motions from overall tumbling. The model-free analysis relates the spectral density to the square of an order parameter, S^2, and an internal effective correlation time, τ_e:

$$J(\omega) = \frac{2}{5}\left[\frac{S^2\tau_m}{1 + \omega^2\tau_m{}^2} + \frac{(1 - S^2)\tau}{1 + \omega^2\tau^2}\right] \quad (4)$$

where $1/\tau = 1/\tau_e + 1/\tau_m$, τ_e measures the time scale of the internal motion, and τ_m is the overall rotational correlation time for isotropic tumbling (*14*, *15*).

S^2, which varies between 0 and 1, indicates the restriction of the motion experienced by a ^{1}H−^{15}N vector. An S^2 value of 0 corresponds to unrestrained isotropic motion with relaxation depending only on τ_e. An S^2 value of 1 corresponds to complete restriction with respect to the molecular frame, which tumbles isotropically with the correlation time corresponding to τ_m. These are model-independent parameters, but they can be used in conjunction with physical models, such as the "wobble-in-a-cone" model (*14*).

Here, we compare the dynamics of apocytochrome b_5 in cells and in dilute solution to assess the influence of the cytosol on these fundamental characteristics of the protein.

MATERIALS AND METHODS

NMR data were acquired at The UNC Biomolecular NMR Laboratory at the University North Carolina on a Varian INOVA spectrometer operating at a ^{1}H frequency of 700 MHz. For in-cell experiments, the sample comprised 90% cell slurry and 10% ^2H_2O (99.9% ^{2}H). For dilute solution experiments, the sample comprised pure ^{15}N-enriched apocytochrome b_5 (~0.5 mM) in 50 mM ionic strength phosphate buffer (pH 7.0) with 10% ^2H_2O. Further details about the {^{1}H}−^{15}N nOe experiments, sample preparation, determining cell survival, and determining the location of apocytochrome b_5 in the in-cell samples are given in our previous work (*8*).

T_2 Experiments. In-cell ^{15}N relaxation measurements were conducted on the 700 MHz Varian spectrometer using a conventional probe. The dilute solution ^{15}N relaxation measurements were carried out on this same instrument with a cryogenic probe. The Varian Bio-pack gNhsqc pulse sequence was used to obtain ^{1}H−^{15}N HSQC spectra (*16*−*18*). The pulse sequence uses gradient selection and leads to minimal water saturation. Spectra were acquired in an interleaved fashion with T_2 relaxation time delays of 0.03, 0.05, 0.09, 0.11, or 0.15 s in random order. To allow the calculation of standard errors, data for each delay time were collected in triplicate.

The total acquisition time for each dilute solution experiment was approximately 14 h. Three 14 h experiments were performed to obtain three independent trials for each of the five delays. The same sample was used for all three dilute solution experiments.

The acquisition time for in-cell experiments was limited to ensure cell viability at the end of each experiment. This regimen requires the use of multiple independent in-cell samples in acquiring the three replicates for each delay time. Quantitative comparison between samples was facilitated by adding a reference spectrum with a very short delay time to each experiment. (Ideally, this reference spectrum would use a 0-s delay time, but we had to use a delay of 0.01 s because this is the shortest delay permitted by the software.) The intensity of each cross-peak in the reference was then used

to normalize the intensity of that cross-peak in the spectra for the other delay times conducted on that sample preparation. The total acquisition time was approximately 47 h for each in-cell experiment. Each experiment comprised two spectra with different delay times and one reference spectrum. Nine 47-h in-cell experiments had to be performed to obtain at least three normalized replicates for each of the five delay times.

T_1 Experiments. Both in-cell and dilute-solution ^{15}N relaxation measurements were conducted on the 700 MHz spectrometer equipped with a cryogenic probe. The Varian Bio-pack gNhsqc pulse sequence was used to obtain ^{1}H−^{15}N HSQC spectra (*16*−*18*). The pulse sequence uses gradient selection and leads to minimal water saturation. Spectra were acquired in an interleaved fashion with varying T_1 relaxation time delays of 0.01, 0.05, 0.20, 0.50, 0.70, and 0.90 s in random order (with 0.01 s conducted as a reference for the in-cell experiments). The regimen for these experiments was similar to that described above for the T_2 experiments, except that each in-cell T_1 experiment (i.e., each sample preparation) comprised a complete set of all delay times and a reference.

Data Processing. The T_1 and T_2 data were processed by first separating the interleaved data using a script written in house. The data sets were then processed independently with NMRPipe (*19*). NMRDraw (*19*) was used to visualize the resulting two-dimensional spectra and analyze cross-peak characteristics. These characteristics (i.e., location, intensity, and width at half-height) were exported into SigmaPlot 8.0 (Systat Software, Inc.). For in-cell experiments, the cross-peak intensities determined for the reference spectrum (0.01 s) were used to normalize the corresponding cross-peaks in the other relaxation delay spectra collected for that sample preparation. Dilute-solution data were not normalized.

T_1. The cross-peak intensities were used to quantify the relaxation time constant for each resolved apocytochrome b_5 cross-peak. The intensities for each residue were plotted versus the relaxation delay time, and the data were fit to the following single exponential with SigmaPlot 8.0:

$$I_t = I_0 e^{-Rt} \quad (5)$$

where I_t is the normalized cross-peak intensity at time t, I_0 is the intensity at time zero, R is the relaxation rate constant ($1/T_1$ or $1/T_2$), and t is the variable relaxation delay time. The T_1 values are the inverse of the weighted average R_1 values from the three trials (*20*). The uncertainty is reported as the standard error (*20*).

T_2. Unlike the in-cell T_1 experiments, each in-cell T_2 experiment did not contain a complete set of relaxation delays; therefore, the average T_2 time constants and associated error were determined as follows. After the cross-peak intensities in each spectrum were normalized, the experiments were separated by relaxation delay, yielding three replicates of each of the five variable delay times. To produce three full sets of data, one value from each of the five delay times was picked at random. These values were combined to produce one full data set. The process was repeated with the remaining data to produce three full data sets. Each five-point data set was then fitted to the single exponential in eq 5 and processed as described for the T_1 data sets.

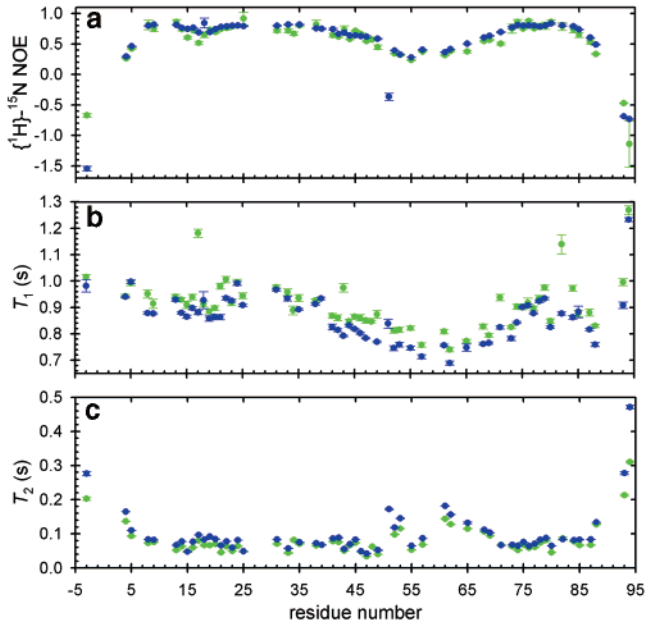

FIGURE 2: Histograms of $\{^1H\}-^{15}N$ nOe (a), T_1 (b), and T_2 (c) in dilute solution (blue) and in living *E. coli* (green). $\{^1H\}-^{15}N$ nOe, T_1, and T_2 values for apocytochrome b_5 were acquired at 700 MHz and 25 °C. Points are the average of three measurements. Vertical bars indicate one standard error. The numbering system is based on the sequence of bovine cytochrome b_5. The nOe data were first published by Bryant et al. (*8*).

RESULTS

Data Sets. T_1, T_2, and nOe data were obtained for 57 ^{15}N−^{1}H pairs in cells and in dilute solution (pH 7.0 and 50 mM phosphate buffer) at a field of 700 MHz and 25 °C. Uncertainties in these measurements were obtained by repeating each experiment three times. Histograms of the T_1, T_2, and nOe data along with their uncertainties are shown in Figure 2. Tables of these data are provided as Supporting Information. Fifty-six of the 57 ^{15}N−^{1}H pairs are common to both the dilute-solution and in-cell data sets. Consistent with our previous study (*8*), approximately 90% of the cells were alive and approximately 90% of the apocytochrome b_5 remained in the cytosol at the end of each experiment. Dilute-solution T_1 data for residues 17 and 82 were inexplicably different from other values. These residues were excluded from analysis.

Analysis of the Data Sets. relxn2.2 (*21*), which utilizes eqs 1−3 and the standard model-free approach (eq 4) to provide values of τ_m, S^2, τ_e, and R_{ex}, was used to analyze the T_1, T_2, and nOe data along with their associated uncertainties. The uncertainties in τ_m, S^2, τ_e, and R_{ex} were estimated by performing 150 steps of Monte Carlo simulation.

The axially symmetric anisotropy of apocytochrome b_5 in solution, calculated on the basis of the NMR ensemble, is 1.2−1.3 (*11*). Complications caused by chemical exchange prevented the application of anisotropic models, and isotropic tumbling was assumed in the original dynamics study (*11*). We make the same assumption because, as shown below, we also observe exchange contributions in cells and in dilute solution. Furthermore, it is unlikely that the shape of the protein changes when it is transferred from dilute solution to the inside of cells because the backbone chemical shifts do not change (*8*).

Table 1: τ_m Values

residues removed	τ_m (ns) dilute solution	τ_m (ns) cells
none	9.6	10.9
those with large-amplitude motions and exchange contributions[a]	9.1	11.1
same as the original study[b]	9.6	10.9
termini and heme binding loop[c]	9.3	10.5
termini and residues with exchange contributions[c]	8.7	10.0

[a] Using the criteria of Tjandra et al. (*23*). [b] From Bhattacharya (*11*). [c] See the text.

Estimating τ_m. Much of apocytochrome b_5 is known to undergo chemical exchange in dilute solution (*11*). The possible influence of exchange on the τ_m obtained from relxn2.2 prompted us to examine the effect of using data from different sets of residues to estimate τ_m. relxn2.2 estimates a global τ_m by minimizing the error function for S^2 and τ_e over a series of τ_m values (*22*).

The results of our analysis are shown in Table 1. The values in the top row are from analysis of all the data. Removing data from residues with large-amplitude internal motions and those subject to chemical exchange using the criteria of Tjandra et al. (*23*) gives the values in the second row. Using the same residue set described in the original dilute-solution analysis of apocytochrome b_5 dynamics (*11*) gives the values shown in the third row. Removing the data for residues in the heme binding loop (residues 40−70) and the termini (*9*) gives the values shown in the fourth row. We also estimated τ_m by removing data for the termini and for residues with significant R_{ex} values. The identification of residues with significant R_{ex} values was accomplished by using the τ_m values from the first row and fitting the data to a model that yields S^2, τ_e, and R_{ex} [model 4 (*24*)]. Residues with R_{ex} values greater than 1 ms^{-1} were removed, and the global τ_m values were determined again. These values are shown in the bottom row of Table 1. Our analysis shows that the choice of residues affects τ_m with values ranging from 8.7 to 9.6 ns in dilute solution and from 10.0 to 11.1 ns in cells. Even though the protein is partially folded, we reach the same conclusion by applying a model that gives a value of τ_m, S^2, and τ_e for each residue (data not shown).

The dilute-solution τ_m values in Table 1 are greater than the value of 5.5 ns from the original study of apocytochrome b_5 dynamics (*11*). To determine the source of this difference, we analyzed the original data using relxn2.2 and the conditions shown in Table 1. Values of between 7.1 and 7.2 ns were obtained. These values are closer to the original value but still approximately 1.5 ns larger. The remaining differences are most likely due to the differences in data sets [two fields in the original study (*11*) vs one here], pH [7.7 (*11*) vs 7.0], buffer [none (*11*) vs 50 mM phosphate], and protein concentration [1 mM (*11*) vs 0.5 mM].

In summary, the choice of residues affects the derived value of τ_m, and our dilute-solution τ_m values are greater than the previously published value. Thus, the τ_m values used here may be, to some extent, ad hoc indicators of the true τ_m values. Despite these potential difficulties, inspection of Table 1 shows that the τ_m in cells is always 1.2−2.0 ns greater than the value in dilute solution.

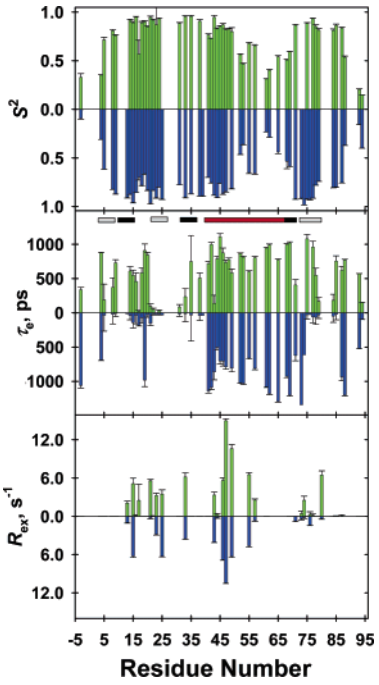

FIGURE 3: Histograms of S^2, τ_e, and R_{ex} with their uncertainties in dilute solution (blue; τ_m = 9.6 ns) and in cells (green; τ_m = 10.9 ns) from fitting the T_1, T_2, and nOe data. The numbering system is based on the sequence of bovine cytochrome b_5. Approximate locations of several elements of secondary structure (*9*) are shown below the top panel (gray for β-strand, black for α-helix, and red for heme-binding loop).

Model-Free Analysis. We used the τ_m values from Table 1 along with the T_1, T_2, and nOe data to estimate values S^2, τ_e, and R_{ex} [model 4 (*24*)]. Histograms of the S^2, τ_e, and R_{ex} values calculated using τ_m-derived values from all the data (top row of Table 1) are shown in Figure 3. Histograms obtained using the τ_m values from the bottom row of Table 1 are shown in Figure 4. Tables of these data are provided as Supporting Information. Typical back-calculated T_1, T_2, and nOe values differ from the experimentally determined values by less than 10%. Despite the small back-calculated errors, the model was unable to provide reasonable parameter values (i.e., negative S^2 values or uncertainties much larger than the value) for some residues. For the histograms in Figure 3, this list comprises residues 13, 25, 73, 74, 76, and 80 in cells and for residue 80 in dilute solution. For the histograms in Figure 4, the list comprises residues 17, 73, and 80 in cells.

To determine if chemical exchange affects S^2 and τ_e, we discarded the T_2 data and used the T_1 and nOe data along with the τ_m values in Table 1 to estimate S^2 and τ_e [model 2 (*24*)]. Histograms obtained using the τ_m values from the top and bottom rows of Table 1 are provided as Supporting Information. Tables of these values are also provided as Supporting Information. Typical back-calculated T_1, T_2, and nOe values differed from the experimentally determined values by much less than 10%. The model was unable to provide reasonable parameter values for certain residues. For the in-cell data fit with a τ_m of 10.9 ns, this list comprises residues 8, 13, 23, 25, 35, 73, 74, 76, 78, 80, and 82. For the dilute-solution data fit with a τ_m of 10.0 ns, this list comprises residue 80. For the in-cell data fit with a τ_m of 10.0 ns, this list comprises residues 73 and 80.

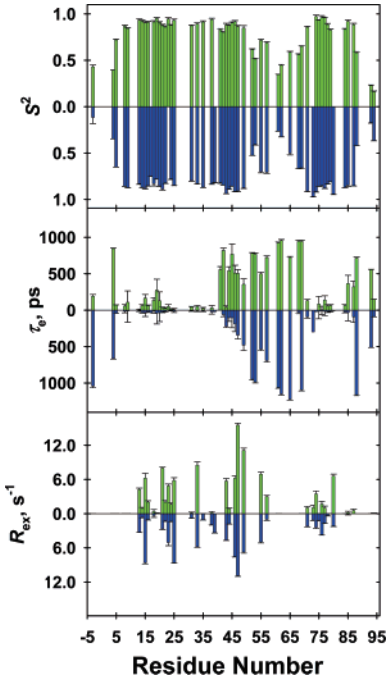

FIGURE 4: Histograms of S^2, τ_e, and R_{ex} with their uncertainties in dilute solution (blue; $\tau_m = 8.7$ ns) and in cells (green; $\tau_m = 10.0$ ns) from fitting the T_1, T_2, and nOe data. The numbering system is based on the sequence of bovine cytochrome b_5.

DISCUSSION

Before analysis of the T_1, T_2, and nOe data shown in Figure 2, it was important to determine if the measured values are quantitatively different in cells versus dilute solution. In our 54-residue data set, 39 nOe values, 43 T_1 values, and 51 T_2 values change by more than the quadratic sum of their respective uncertainties (*20*) when the sample is transferred from dilute solution to the cytosol. This observation means that further analysis to uncover the source of these differences is warranted.

The Cytosol Is More Viscous than Dilute Solution. Comparing pairs of τ_m values from Table 1 shows that transfer of the protein into cells increases τ_m by approximately 10%. This observation is consistent with inspection of Figure 2, which shows that nearly all the in-cell T_1 values are greater than their respective dilute-solution values. Using the Stokes−Einstein equation, we conclude that the cytosol is approximately 10% more viscous than water. This increase is consistent with a study showing that viscosity is no more than doubled in cells compared to that in dilute solution (*25*). As discussed below, this increased viscosity accounts for most of the differences in dynamic behavior.

No Effect on the Amplitude of Picosecond to Nanosecond Backbone Motion. Figures 3 and 4 show histograms of S^2, τ_e, and R_{ex} in cells (green) and in dilute solution (blue). S^2, τ_e, and R_{ex} were determined by using the τ_m values from the top (Figure 3) and bottom (Figure 4) rows of Table 1. The horizontal bars below the top panel delineate the secondary structural features of the protein (*9*). The average values of S^2, τ_e, and R_{ex} for the six panels in Figures 3 and 4, along with their respective average standard deviations, are listed in Table 2.

The top panels of Figures 3 and 4 show S^2, the amplitude of the fast motions. As observed in the original study (*11*), the regions of α-helix and β-sheet tend to exhibit some of the largest values, while the termini and the C-terminal portion of the heme-binding loop exhibit smaller values. These patterns are independent of the large chemical-exchange contribution to T_2 (ref *11* and vide infra) because we observe exactly the same patterns if we delete the T_2 data and fit the T_1 and nOe data to a model that yields only S^2 and τ_e (see the Supporting Information).

Table 2: Average Dynamic Parameters with Average Standard Deviations from Model-Free Analysis of T_1, T_2, and nOe Data Using τ_m Values from Table 1

	dilute solution	cells
τ_m (ns)	9.6	10.9
S^2	0.71 ± 0.01	0.74 ± 0.03
τ_e (ps)	460 ± 40	600 ± 60
R_{ex} (s^{-1})	1.1 ± 0.1	1.7 ± 0.2
τ_m (ns)	8.7	10.0
S^2	0.73 ± 0.01	0.73 ± 0.01
τ_e (ps)	260 ± 10	330 ± 40
R_{ex} (s^{-1})	1.7 ± 0.1	2.3 ± 0.2

Most importantly, the pattern of S^2 values (Figures 3 and 4) is the same in dilute solution and in cells. As shown in Table 2, the average values of S^2 are also the same to within the measured uncertainty. The fact that S^2 is independent of viscosity shows that the internal motions being probed are independent of the overall molecular tumbling. We conclude that the transfer of the protein from dilute solution into the cytosol does not change the amplitude of picosecond to nanosecond backbone dynamics. This lack of change was also observed in a study of the cold shock protein in the presence of the small molecule crowding agent, ethylene glycol (*26*).

The Cytosol Slightly Increases the Time Scale of Picosecond to Nanosecond Backbone Motions. The middle panels of Figures 3 and 4 show histograms of τ_e as a function of residue number. The pattern of the dilute solution data shows that the heme-binding loop exhibits motion on the time scale of hundreds of picoseconds, while regions of defined secondary structure tend to have τ_e values of tens of picoseconds. Both observations are consistent with the original study (*11*).

Inspection of Figures 3 and 4 shows that transferring the protein into cells has an only small effect on τ_e in the heme-binding loop and at the termini, but there is a general increase in τ_e outside these regions. The data in Table 2 indicate an average increase in τ_e of 10−30%. Deeper analysis of these data is not warranted for several reasons. First, τ_e is not as well determined as S^2 when data from only one magnetic field strength are used (*27*). Second, the increase in τ_e outside the loop and termini is diminished when we use smaller τ_m values (compare Figures 3 and 4). Additionally, τ_e is sensitive to errors in τ_m and anisotropy effects.

We conclude that transfer into cells does not affect τ_e in less structured regions but slightly increases the value in regions of defined secondary structure. The most straightforward interpretation for the slight increase is that these internal motions are affected by viscosity in the same way as overall tumbling (τ_m, vide supra) is affected by viscosity.

The Cytosol Slightly Lengthens the Time Scale of Microsecond to Millisecond Motions. The bottom panels of Figures 3 and 4 show histograms of R_{ex} as a function of residue number. Consistent with the original study of apocytochrome

b_5 dynamics (*11*), residues undergoing chemical exchange are observed throughout the protein. Transfer into the cytosol does not affect the pattern of R_{ex} values, but as shown in Table 2, the average value of R_{ex} increases when the protein is transferred into cells. The observation that transfer to the cytosol does not dampen slower dynamic processes is consistent with the observation that the crowded environment in cells does not lead to the formation of additional stable structure in apocytochrome b_5 (*8*).

Deeper analysis is not warranted because R_{ex} is calculated as a "fudge factor" to bring T_2 values in line with S^2 and τ_e. More detailed information about the cytosol's effect on slower motions will require the application of direct methods such as those involving $R_{1\rho}$- or CPMG-based experiments (*28*, *29*). In-cell relaxation studies, however, will be limited by practical considerations such as cell viability. Although the full complement of experiments typically used to characterize local motions and slow processes was not performed, our semiquantitative analysis, assuming a conservation of anisotropic properties, does not reveal a large influence of the cellular milieu.

Summary and Implications. Transfer to the cytosol has a quantitative effect on T_1, T_2, and the nOe of apocytochrome b_5. Almost all these changes can be attributed to an increase in the overall correlation time caused by the increased viscosity of the cytosol compared to that of dilute solution. Our main conclusion is that the cytosol does not alter the pattern of backbone dynamics of apocytochrome b_5. We do observe quantitative increases in the time scale of both the picosecond and millisecond motions, but the increases are less than ~30%.

Our system for studying backbone dynamics requires overexpression of a recombinant protein in *E. coli*, which leads to questions about the physiological significance of our conclusions. We estimate that the intracellular concentration of apocytochrome b_5 is in the millimolar range, which is approximately 100 times the concentration of the most abundantly expressed soluble protein in wild-type *E. coli* cells (*30*). Nevertheless, there are three reasons to believe our conclusions are physiologically relevant and generally applicable. First, overexpression does not alter the total cellular protein concentration (*2*). Second, any other (unknown) effects of overexpression are seemingly irrelevant because we observe no change in the pattern of dynamic behavior. Third, using apocytochrome b_5 allowed us to assess backbone dynamics over a broad time scale, from picoseconds to milliseconds.

ACKNOWLEDGMENT

We thank Jillian Orans and Denise Teotico for help with Figure 1, Nancy Scott for plasmid preparation, and Michael "Sparky" Clarkson for help with the relxn2.2 visual interface. G.J.P. thanks David Goldenberg and Elizabeth Pielak for helpful discussions. We also thank the referees for suggesting a more quantitative approach to data analysis.

SUPPORTING INFORMATION AVAILABLE

Tables and histograms of the nOe, T_1, T_2, S^2, τ_e, and R_{ex} values. This material is available free of charge via the Internet at http://pubs.acs.org.

REFERENCES

1. Luby-Phelps, K. (2000) Cytoarchitecture and physical properties of cytoplasm: Volume, viscosity, diffusion, intracellular surface area, *Int. Rev. Cytol. 192*, 189−221.
2. Dedmon, M. M., Patel, C. N., Young, G. B., and Pielak, G. J. (2002) FlgM gains structure in living cells, *Proc. Natl. Acad. Sci. U.S.A. 99*, 12681−12684.
3. McNulty, B. C., Young, G. B., and Pielak, G. J. (2006) Macromolecular crowding in the *Escherichia coli* periplasm maintains α-synuclein disorder, *J. Mol. Biol. 355*, 893−897.
4. Rivas, G., Fernandez, J. A., and Minton, A. P. (2001) Direct observation of the enhancement of noncooperative protein self-assembly by macromolecular crowding: Indefinite linear self-association of bacterial cell division protein FtsZ, *Proc. Natl. Acad. Sci. U.S.A. 98*, 3150−3155.
5. Sasahara, K., McPhie, P., and Minton, A. P. (2003) Effect of dextran on protein stability and conformation attributed to macromolecular crowding, *J. Mol. Biol. 326*, 1227−1237.
6. Serber, Z., Corsini, L., Durst, F., and Dötsch, V. (2005) In-cell NMR spectroscopy, *Methods Enzymol. 394*, 17−41.
7. Serber, Z., Ledwidge, R., Miller, S. M., and Dötsch, V. (2001) Evaluation of parameters critical to observing proteins inside living *Escherichia coli* by in-cell NMR spectroscopy, *J. Am. Chem. Soc. 123*, 8895−8901.
8. Bryant, J. E., Lecomte, J. T. J., Lee, A. L., Young, G. B., and Pielak, G. J. (2005) Protein dynamics in living cells, *Biochemistry 44*, 9275−9279.
9. Falzone, C. J., Mayer, M. R., Whiteman, E. L., Moore, C. D., and Lecomte, J. T. J. (1996) Design challenges for hemoproteins: The solution structure of apocytochrome b_5, *Biochemistry 35*, 6519−6526.
10. Falzone, C. J., Wang, Y., Vu, B. C., Scott, N. L., Bhattacharya, S., and Lecomte, J. T. J. (2001) Structural and dynamic perturbations induced by heme binding in cytochrome b_5, *Biochemistry 40*, 4879−4891.
11. Bhattacharya, S., Falzone, C. J., and Lecomte, J. T. J. (1999) Backbone dynamics of apocytochrome b_5 in its native, partially folded state, *Biochemistry 38*, 2577−2589.
12. Abragam, A. (1961) *The Principles of Nuclear Magnetism*, Clarendon Press, Oxford, U.K.
13. Palmer, A. G., III (2001) NMR probes of molecular dynamics: Overview and comparison with other techniques, *Annu. Rev. Biophys. Biomol. Struct. 30*, 129−155.
14. Lipari, G., and Szabo, A. (1982) Model-free approach to the interpretation of nuclear magnetic resonance relaxation in macromolecules. 1. Theory and range of validity, *J. Am. Chem. Soc. 104*, 4546−4559.
15. Lipari, G., and Szabo, A. (1982) Model-free approach to the interpretation of nuclear magnetic resonance relaxation in macromolecules. 2. Analysis of experimental results, *J. Am. Chem. Soc. 104*, 4559−4570.
16. Kay, L. E., Nicholson, L. K., Delaglio, F., Bax, A., and Torchia, D. A. (1992) Pulse sequences for removal of the effects of cross correlation between dipolar and chemical-shift anisotropy relaxation mechanisms on the measurement of heteronuclear T_1 and T_2 values in proteins, *J. Magn. Reson. 97*, 359−375.
17. Kay, L. E., Keifer, P., and Saarinen, T. (1992) Pure absorption gradient enhanced heteronuclear single quantum correlation spectroscopy with improved sensitivity, *J. Am. Chem. Soc. 114*, 10663−10665.
18. Farrow, N. A., Muhandiram, R., Singer, A. U., Pascal, S. M., Kay, C. M., Gish, G., Shoelson, S. E., Pawson, T., Forman-Kay, J. D., and Kay, L. E. (1994) Backbone dynamics of a free and a phosphopeptide-complexed Src homology 2 domain studied by ^{15}N NMR relaxation, *Biochemistry 33*, 5984−6003.
19. Delaglio, F., Grzesiek, S., Vuister, G. W., Zhu, G., Pfeifer, J., and Bax, A. (1995) NMRPipe: A multidimensional spectral processing system based on UNIX pipes, *J. Biomol. NMR 6*, 277−293.
20. Taylor, J. R. (1982) *An Introduction to Error Analysis*, 2nd ed., University Science Books, Sausalito, CA.
21. Lee, A. L., and Wand, A. J. (1999) Assessing potential bias in the determination of rotational correlations times of proteins by NMR, *J. Biomol. NMR 13*, 101−112.
22. Dellwo, M. J., and Wand, A. J. (1989) Model-independent and model-dependent analysis of the global and internal dynamics of cyclosporin A, *J. Am. Chem. Soc. 111*, 4571−4578.

23. Tjandra, N., Feller, S. E., Pastor, R. W., and Bax, A. (1995) Rotational diffusion anisotropy of human ubiquitin from ^{15}N NMR relaxation, *J. Am. Chem. Soc. 117*, 12562−12566.
24. Jarymowycz, V. A., and Stone, M. J. (2006) Fast time scale dynamics of protein backbones: NMR relaxation methods, applications, and functional consequences, *Chem. Rev. 106*, 1624−1671.
25. Williams, S. P., Haggie, P. M., and Brindle, K. M. (1997) ^{19}F NMR measurements of the rotational mobility of proteins, *Biophys. J. 72*, 490−498.
26. Zeeb, M., Jacob, M. H., Schindler, T., and Balbach, J. (2003) ^{15}N relaxation of the cold shock protein CspB at various solvent viscosities, *J. Biomol. NMR 27*, 221−234.
27. Ernst, R. R., Blackledge, M. J., Bremi, T., Brüshweiler, R., Ernst, M., Griesinger, C., Mádi, Z. L., Peng, J. M., Schmid, J. M., and Xu, P. (1996) in *NMR as a Structural Tool for Macromolecules: Current Status and Future Directions* (Nageswara Rao, B. D. N., and Kempleeds, M. D., Eds.) pp 15−30, Plenum Press, New York.
28. Palmer, A. G., III (2004) NMR characterization of the dynamics of biomacromolecules, *Chem. Rev. 104*, 3623−3640.
29. Mittermaier, A., and Kay, L. E. (2006) New tools provide new insights in NMR studies of protein dynamics, *Science 312*, 224−228.
30. Pedersen, S., Bloch, P. L., and Neidhardt, F. C. (1978) Patterns of protein expression in *E. coli*: A catalog of the amount of 140 individual proteins at different growth rates, *Cell 14*, 179−190.
31. DeLano, W. L. (2005) *MacPyMOL: A PyMOL-based Molecular Graphics Application for MacOS X*, DeLano Scientific LLC, South San Francisco, CA (http://www.pymol.org).

BI060547B